Electronic Supplementary Information

First-principles-based Microkinetic Modeling of Methanol Steam Reforming over Cu(111) and Cu(211): Structure Sensitive Activity and Selectivity

Xinyi Zhang and Bo Yang*

School of Physical Science and Technology, ShanghaiTech University, 393 Middle Huaxia Road, Shanghai 201210, China

*E-mail: yangbo1@shanghaitech.edu.cn

Table S1. Activation energies (E_a) and reaction energies (ΔE), in eV, for the all elementary steps in the full reaction network of methanol steam reforming to CO and CO_2 on Cu(211) and Cu(111).

Elementary steps	Cu(111)		Cu(211)	
	E_a	ΔE	E_a	ΔE
2* + CH_3OH_g → CH_3O* + H*	1.03	-0.31	1.03	-0.36
CH_3* + OH* → CH_3OH* + *	1.89	-0.06	2.13	0.22
CH_3OH* + * → CH_2OH* + H*	1.67	1.06	1.71	0.90
H_2O_g + 2* → OH* + H*	1.20	-0.17	1.14	-0.35
OH* + * → O* + H*	1.82	0.63	1.76	0.94
CH_3O* + * → H* + CH_2O*	1.42	0.99	1.28	1.10
CH_3O* + * → CH_3* + O*	1.92	0.71	1.97	0.74
CH_3* + * → CH_2* + H*	1.60	0.88	1.38	1.05
CH_2* + * → CH* + H*	1.11	0.45	0.84	0.24
CH* + * → C* + H*	2.02	1.27	1.57	0.88
CH_2* + OH* → CH_2OH* + *	1.24	0.12	0.97	0.08
CH_2OH* + * → CH_2O* + H*	1.09	-0.09	1.29	0.18
CH_2OH* + * → CHOH* + H*	1.03	0.54	0.99	0.64
CHOH* + * → HCO* + H*	0.75	-0.26	1.06	-0.18
HCO* + * → CO* + H*	0.31	-0.75	0.38	-0.42
CHOH* + * → COH* + H*	0.92	0.21	1.24	0.60
COH* + * → CO* + H*	1.23	-1.21	0.70	-1.20
CH_2O* + * → CH_2* + O*	1.52	0.60	1.48	0.68
CH_2O* + * → HCO* + H*	0.96	0.38	1.00	0.28
CH_2O* + OH* → H_2COOH* + *	0.16	-0.42	0.04	-0.40
H_2COOH* + * → HCOOH* + H*	1.08	-0.02	1.07	0.29
H_2COOH* + * → H_2COO* + H*	1.45	0.39	1.53	0.35
HCOOH* + * → HCOO* + H*	0.71	-0.39	0.69	-0.66
HCOO* + * → CO_2_g + H* + *	1.19	0.70	1.52	1.14
CO* + O* → CO_2_g + 2*	0.73	-0.38	0.30	-0.45
HCO* + O* → HCOO* + *	0.34	-1.83	0.58	-2.01
H_2COO* + * → HCOO* + H*	0.89	-0.79	0.96	-0.73
COOH* + H* → HCOOH* + *	0.91	-0.48	0.85	-0.37

$COOH^* + * \rightarrow CO_2\_g + H^* + *$	1.39	-0.17	1.81	0.11
$CO^* + OH^* \rightarrow COOH^* + *$	0.72	0.42	0.90	0.39
$COH^* + O^* \rightarrow COOH^* + *$	0.81	-1.42	1.39	-1.76
$HCO^* + OH^* \rightarrow HCOOH^* + *$	0.69	-0.82	1.76	-0.40
$CH_2O^* + O^* \rightarrow H_2COO^* + *$	0.02	-0.66	0.04	-0.99
$CH^* + OH^* \rightarrow CHOH^* + *$	1.31	0.21	1.76	0.48
$CH^* + O^* \rightarrow HCO^* + *$	1.08	-0.67	1.32	-0.64
$C^* + OH^* \rightarrow COH^* + *$	1.23	-0.85	2.34	0.20
$C^* + O^* \rightarrow CO^* + *$	1.17	-2.69	1.46	-1.94
$H_2COOH^* + * \rightarrow CH_2OH^* + O^*$	1.74	1.14	2.18	1.16
$CHOH^* + O^* \rightarrow HCOOH^* + *$	0.34	-1.70	0.55	-1.52
$CH_2O^* + CH_3O^* \rightarrow CH_2OOCH_3^* + *$	0.24	-0.43	0.10	-0.57
$CH_2OOCH_3^* + * \rightarrow H_2COO^* + CH_3^*$	2.03	0.48	2.25	0.32
$CH_2OOCH_3^* + * \rightarrow HCOOCH_3^* + H^*$	1.01	0.02	1.17	0.32
$HCOOCH_3^* + * \rightarrow HCOOCH_2^* + H^*$	1.75	0.91	1.72	0.67
$HCOOCH_3^* + OH^* \rightarrow HOOHCOCH_3^* + *$	0.56	0.27	0.70	0.23
$HOOHCOCH_3^* + * \rightarrow HCOOOCH_3^* + H^*$	1.40	0.42	1.70	0.48
$HCOOOCH_3^* + * \rightarrow HCOO^* + CH_3O^*$	0.19	-1.10	0.27	-1.25
$HCOOCH_3^* + * \rightarrow HCO^* + CH_3O^*$	1.38	0.79	1.48	0.53
$HCOOCH_2^* + * \rightarrow HCOO^* + CH_2^*$	0.76	-0.36	0.99	-0.37
$HCOOCH_3^* + * \rightarrow HCOO^* + CH_3^*$	1.50	-0.33	1.33	-0.74
$HCOOOCH_3^* + * \rightarrow HCOOCH_3^* + O^*$	0.35	-0.06	0.38	0.23
$HOOHCOCH_3^* + * \rightarrow HCOOH^* + CH_3O^*$	0.37	-0.29	0.38	-0.10
$H^* + H^* \rightarrow H_2\_g + 2^*$	0.96	0.27	0.95	0.15
$CO^* \rightarrow CO\_g + *$	-	0.55	-	0.50

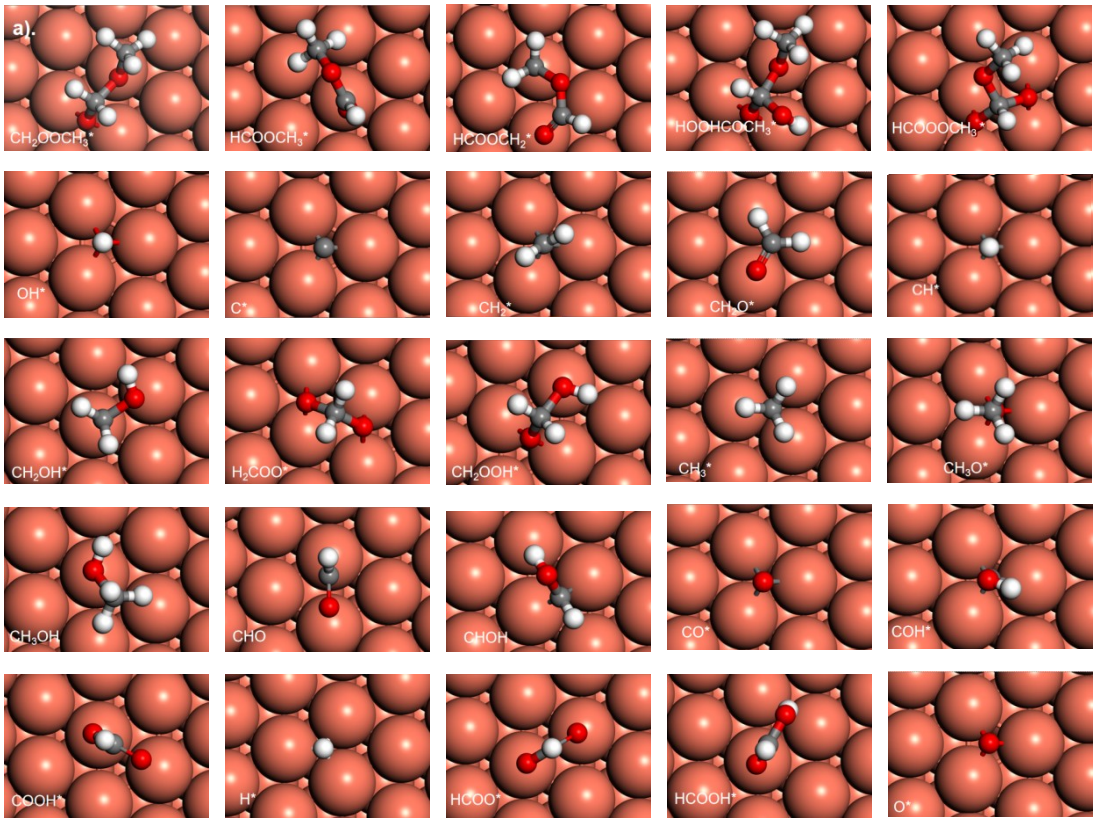
a).
CH_2OOCH_3*
$HCOOCH_3$*
$HCOOCH_2$*
$HOOHCOCH_3$
$HCOOOCH_3$*
OH*
C*
CH_2*
CH_2O*
CH*
CH_2OH*
H_2COO*
CH_2OOH*
CH_3*
CH_3O*
CH_3OH
CHO
CHOH
CO*
COH*
COOH*
H*
HCOO*
HCOOH*
O*

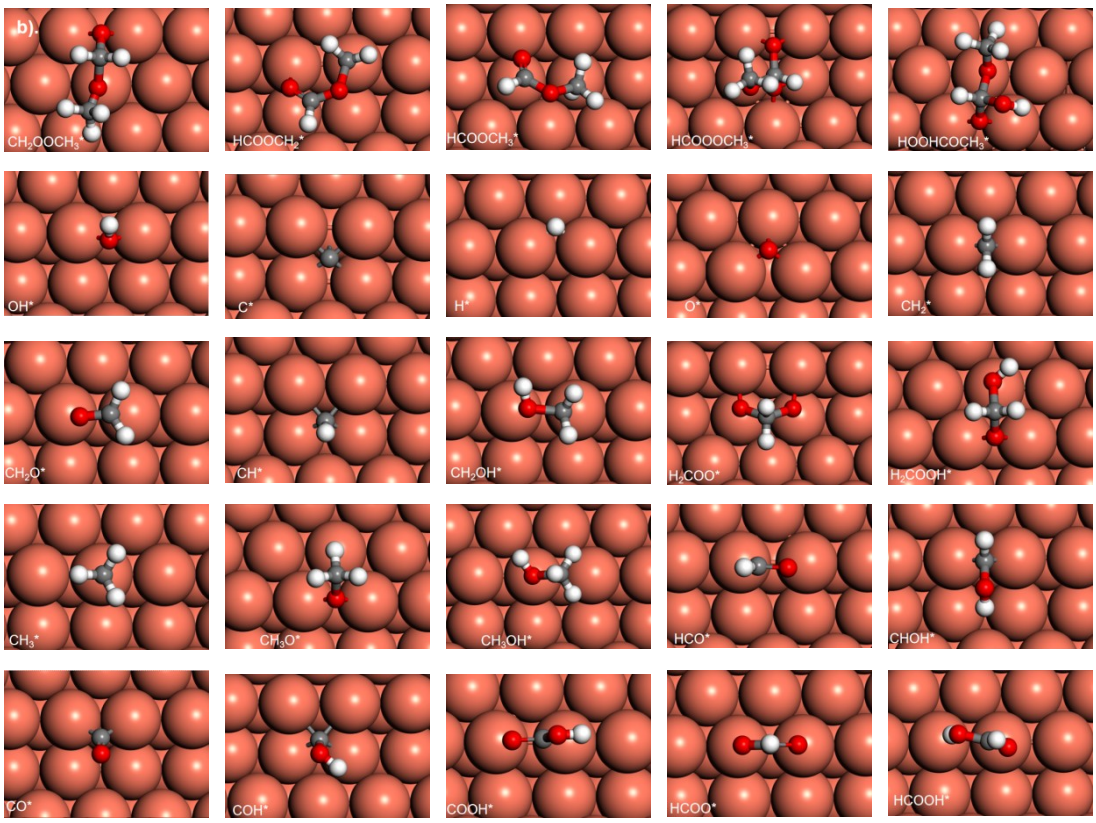
b).
CH_2OOCH_3*
$HCOOCH_2$*
$HCOOCH_3$*
$HCOOOCH_3$*
$HOOHCOCH_3$*
OH*
C*
H*
O*
CH_2*
CH_2O*
CH*
CH_2OH*
H_2COO*
H_2COOH*
CH_3*
CH_3O*
CH_3OH*
HCO*
CHOH*
CO*
COH*
COOH*
HCOO*
HCOOH*

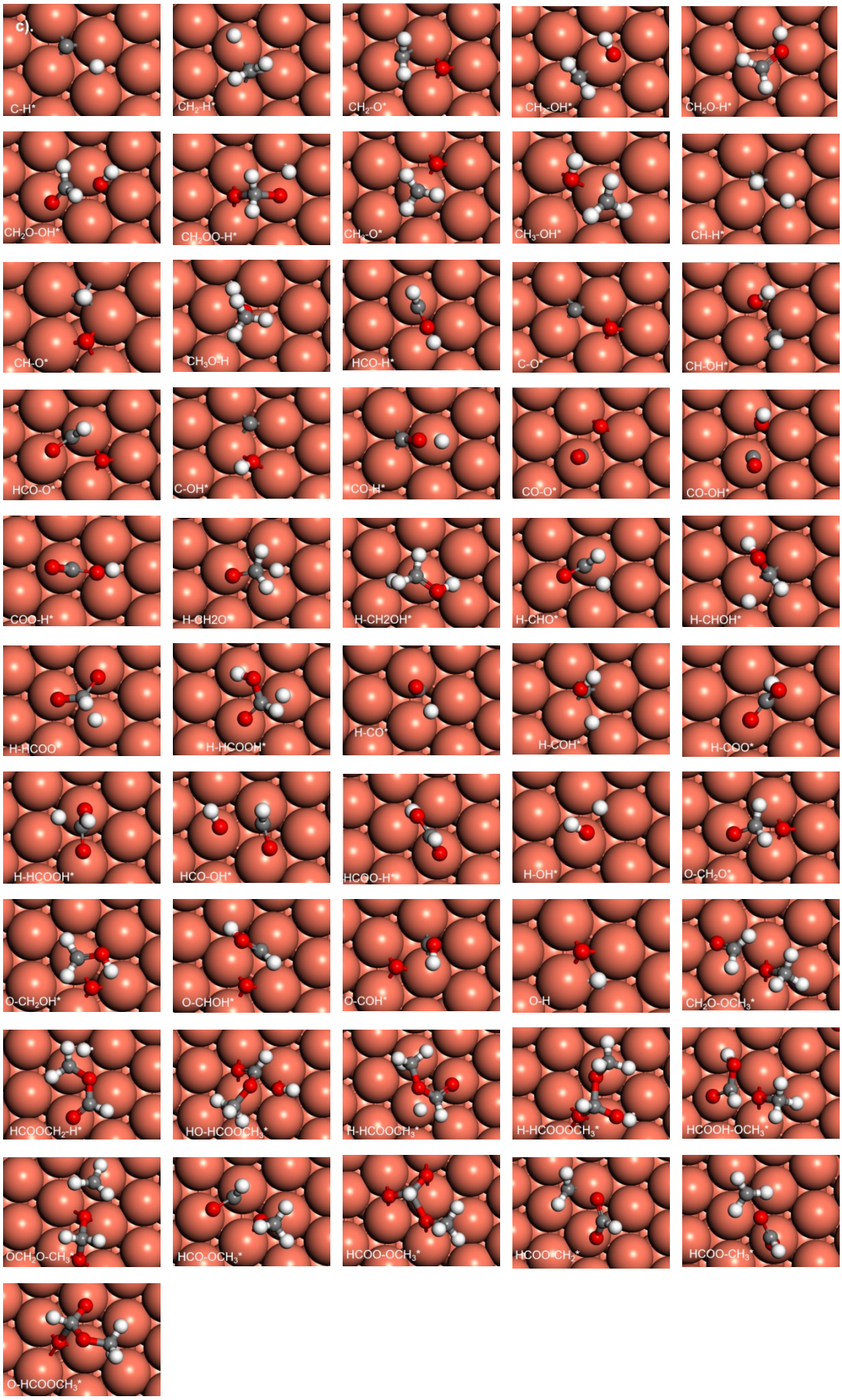
c).
C-H*
CH2-H*
CH2-O*
CH2-OH*
CH2O-H*
CH2O-OH*
CH2OO-H*
CH2-O*
CH3-OH*
CH-H*
CH-O*
CH3O-H
HCO-H*
C-O*
CH-OH*
HCO-O*
C-OH*
CO-H*
CO-O*
CO-OH*
COO-H*
H-CH2O*
H-CH2OH*
H-CHO*
H-CHOH*
H-HCOO*
H-HCOOH*
H-CO*
H-COH*
H-COO*
H-HCOOH*
HCO-OH*
HCOO-H*
H-OH*
O-CH2O*
O-CH2OH*
O-CHOH*
O-COH*
O-H
CH2O-OCH3*
HCOOCH2-H*
HO-HCOOCH3*
H-HCOOCH3*
H-HCOOOCH3*
HCOOH-OCH3*
OCH2O-CH3*
HCO-OCH3*
HCOO-OCH3*
HCOO-CH2*
HCOO-CH3*
O-HCOOCH3*

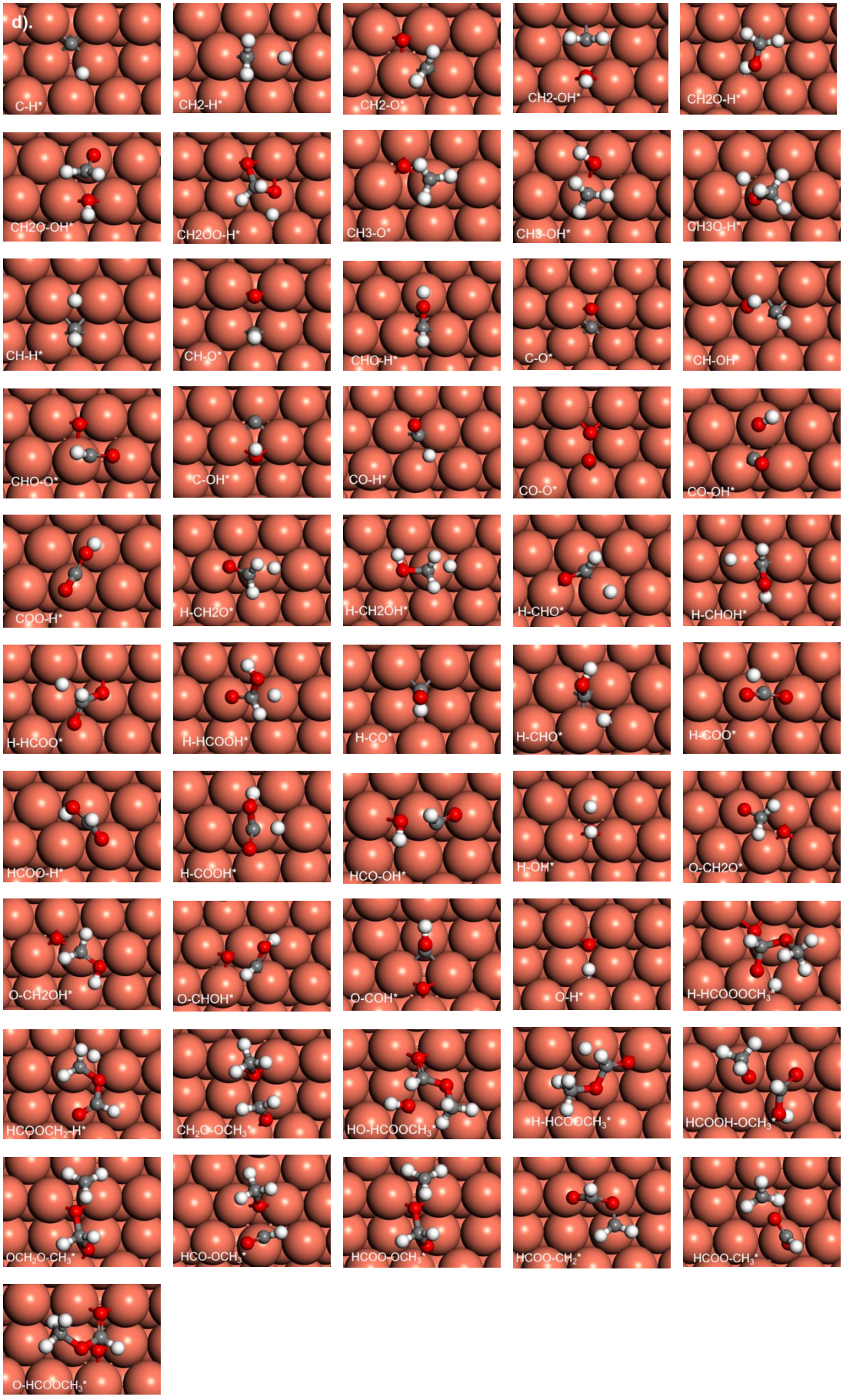
d).
C-H*
CH2-H*
CH2-O*
CH2-OH*
CH2O-H*
CH2O-OH*
CH2OO-H*
CH3-O*
CH3-OH*
CH3O-H*
CH-H*
CH-O*
CHO-H*
C-O*
CH-OH*
CHO-O*
C-OH
CO-H*
CO-O*
CO-OH*
COO-H*
H-CH2O*
H-CH2OH*
H-CHO*
H-CHOH*
H-HCOO*
H-HCOOH*
H-CO*
H-CHO*
H-COO*
HCOO-H*
H-COOH*
HCO-OH*
H-OH*
O-CH2O*
O-CH2OH*
O-CHOH*
O-COH*
O-H*
H-HCOOOCH3*
HCOOCH2-H*
CH2O-OCH3*
HO-HCOOCH3
H-HCOOCH3*
HCOOH-OCH3*
OCH2O-CH3*
HCO-OCH3*
HCOO-OCH3*
HCOO-CH2*
HCOO-CH3*
O-HCOOCH3*

Figure S1. The optimized structures of (a) surface intermediates over Cu(111), (b) surface intermediates over Cu(211), (c) transition states over Cu(111), and (d) transition states over Cu(211).

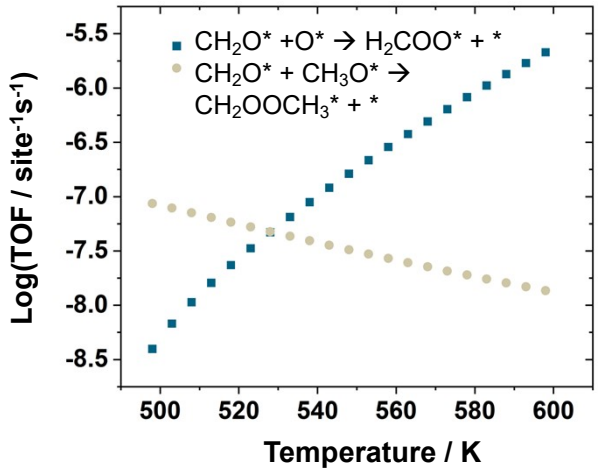

Figure S2. The variation of reaction rates of two elementary steps under S:M = 0.1.

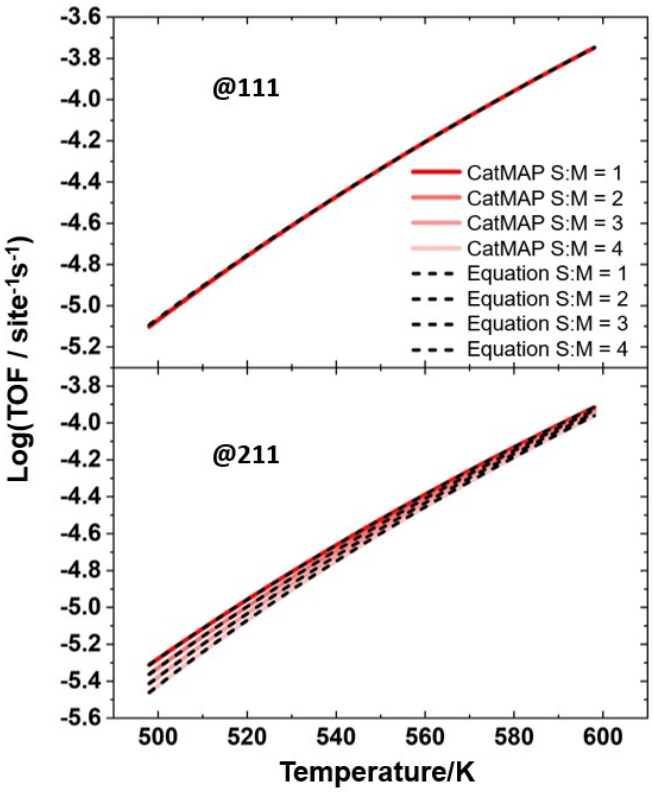

Figure S3. Reaction rates calculated by rate equations compared to those calculated with CatMAP.

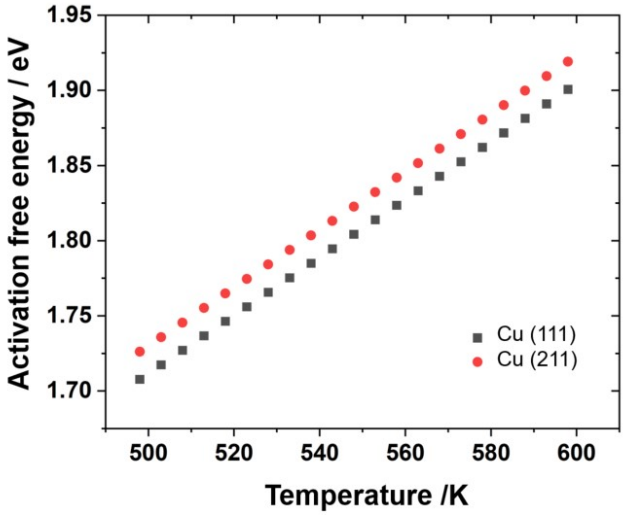

Figure S4. Activation free energies of methanol dehydrogenation to methoxy over Cu(211) and Cu(111) as a function of temperature.

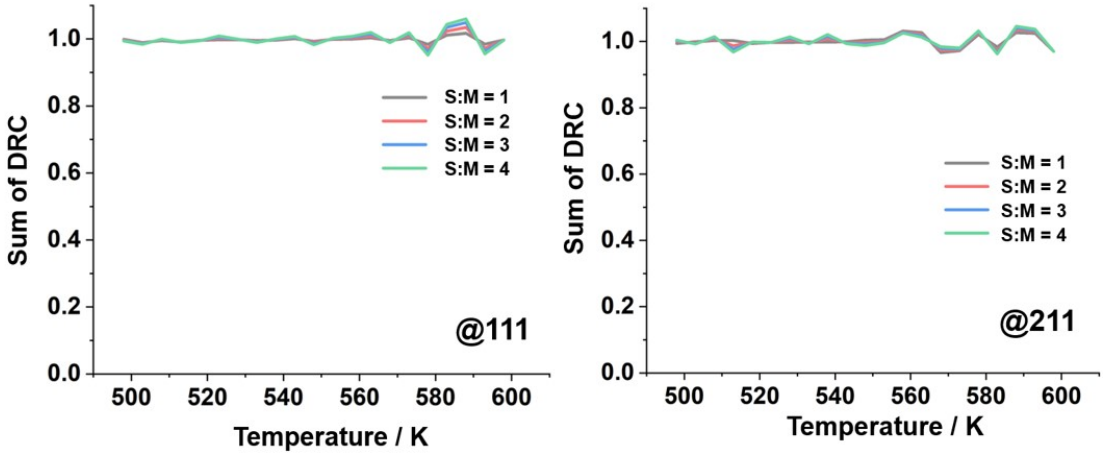

Figure S5. Sum of DRC values of all transition states at different temperatures over Cu(211) and Cu(111).

According to the established definitions, the reaction order can be expressed mathematically as $\sum_i (\partial(lnr)/\partial(ln\, p_i))$, while the apparent activation energy is represented as $\partial(ln\, r)/\partial(-1/(k_B T))$. Furthermore, we have identified that the dissociative adsorption of methanol constitutes the rate-controlling step. Consequently, the rate can be described by the equation $Ae^{-G_a/k_B T} p_{CH_3OH} \theta_*^2$. It is noteworthy that the disparity in reaction orders observed over the Cu(111) and Cu(211) surfaces primarily arises from the term θ_*^2 at the same CH_3OH partial pressures. In contrast, the difference between the apparent activation energies is determined by both G_a and θ_*^2. According to Section 3.3, the predominant surface species across the entire temperature range is hydroxyl. Therefore, we can theoretically derive the relationship between the coverage of free sites and steam partial pressure (p_{steam}) by assuming that hydroxyl (OH) and hydrogen (H) are the only adsorbates present on the surface. The relevant reactions can be represented as follows:

$$H_2O(g) + 2* \rightarrow H* + OH* \quad K_1$$

$$H* \rightarrow \frac{1}{2}H_2(g) + * \quad K_2$$

Given that the dissociative adsorption of methanol is the rate-controlling step, the remaining elementary steps can be treated as quasi-equilibrium processes. Thus, we can express the coverage θ_* as follows:

$$\theta_* = \frac{\sqrt{p_{H_2}}/K_2}{\sqrt{p_{H_2}}/K_2 + K_1 p_{steam}}$$

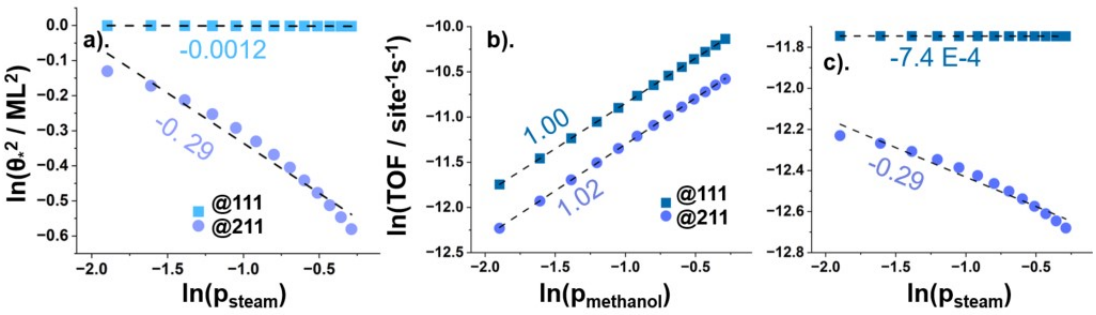

Figure S6. (a) The values of $ln\, \theta_*^2$ against ln(p_{steam}) at T = 498 K and p = 1 bar. (b~c)

The reaction orders calculated from CatMAP data against ln($p_{methanol}$) and ln(p_{steam}), respectively.

We first plotted the values of $ln\,\theta_*^2$ against ln(p_{steam}) at T = 498 K and p = 1 bar in Figure S6 (a). The results of the linear fitting indicate that the slopes are approximately -0.001 for Cu(111) and -0.3 for Cu(211). The reaction orders calculated from CatMAP data are presented in Figure S6 (b,c), where $lnTOF$ is plotted against $ln\,p_i$ under the same conditions. It is evident that the reaction order closely aligns with the results derived from the slope of the $ln\,\theta_*^2$-ln(p_{steam}) plot. This analysis leads to the conclusion that the reaction order over Cu(111) is 1, whereas for Cu(211), it is 0.73.

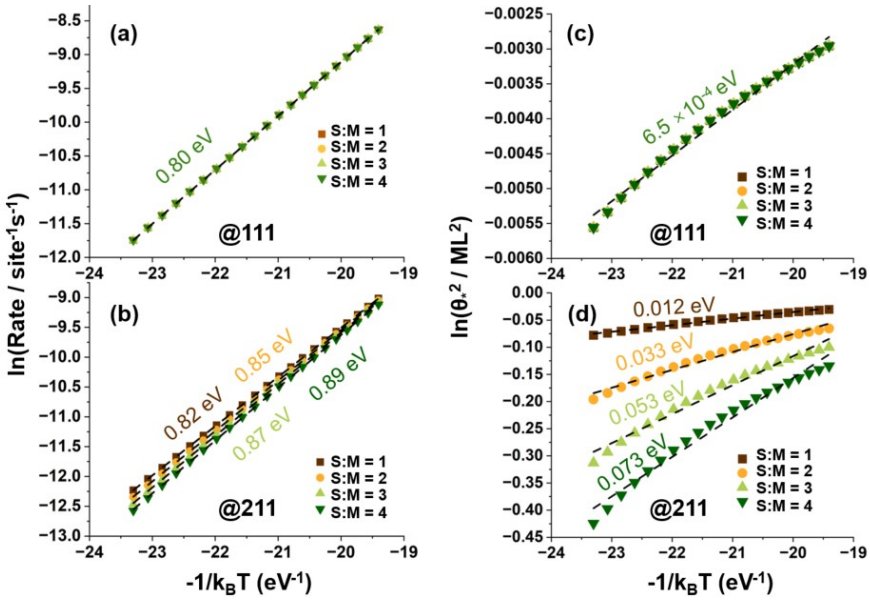

Figure S7. (a~b) Plot of $ln\,r$ against $-1/(k_BT)$. (c~d) $ln\,\theta_*^2$ plotted against $-1/(k_BT)$.

We then plotted $ln\,r$ against $-1/(k_BT)$ in Figure S7 (a) and (b). It is observed that over Cu(111), the apparent activation energy remains constant across varying S:M ratios, while for Cu(211), the apparent activation energy decreases as the S:M ratio increases. The results of $ln\,\theta_*^2$ plotted against $-1/(k_BT)$ are presented in Figure S7 (c) and (d). In Figure S7 (c), the value of $\partial(ln\,\theta_*^2)/\partial(-1/(k_BT))$ is 0.00065 eV, whereas in Figure S7 (d), this value is significantly larger and increases with the S:M ratio. This indicates

that the coverage of free sites over the Cu(211) facet exhibits greater variability compared to the Cu(111) facet. The activation energies of the rate-controlling step calculated via DFT are both 1.03 eV for the Cu(111) and Cu(211) facets, suggesting that the contribution of G_a on the apparent activation energies is nearly identical across these two surfaces. We can conclude that the observed difference in the value of $\partial(ln\,\theta_*^2)/\partial(-1/(k_BT))$ accounts for the differing apparent activation energies between Cu(111) and Cu(211), as well as the variation observed over Cu(211) under different S:M ratios.